Cycling and floating performance of symmetric supercapacitor derived from coconut shell biomass

Cite as: AIP Advances **6**, 115306 (2016); https://doi.org/10.1063/1.4967348
Submitted: 27 August 2016 • Accepted: 24 October 2016 • Published Online: 01 December 2016

Farshad Barzegar, Abubakar A. Khaleed, Faith U. Ugbo, et al.

Cycling and floating performance of symmetric supercapacitor derived from coconut shell biomass

Farshad Barzegar, Abubakar A. Khaleed, Faith U. Ugbo, Kabir O. Oyeniran, Damilola Y. Momodu, Abdulhakeem Bello, Julien K. Dangbegnon, and Ncholu Manyala[a]

Department of Physics, Institute of Applied Materials, SARCHI Chair in Carbon Technology and Materials, University of Pretoria, Pretoria 0028, South Africa

(Received 27 August 2016; accepted 24 October 2016; published online 2 November 2016)

This work present two-step synthesizes route to low-cost mesoporous carbon from coconut shell. The electrochemical characterization of the coconut shell based activated carbon (CSAC) material as electrode for supercapacitor showed a specific capacitance of 186 F g^{-1}, energy density of ~11 Wh kg^{-1} and power density of 325 W kg^{-1} at a 0.5 A g^{-1} with an excellent stability after floating for 100 h and cycling for 10000 cycles in polymer gel electrolyte. The CSAC showed very good potential as a stable material for supercapacitors desirable for high power applications. [http://dx.doi.org/10.1063/1.4967348]

I. INTRODUCTION

Supercapacitors utilize charge separation mechanisms to propagate high power delivery when compared with other storage technologies such as batteries which store energy in chemical form. This makes them suitable for transient energy saving application such as energy capture during braking in vehicles, in construction equipment such as cranes and for the opening of doors in the A380 Jumbo jet. Supercapacitors are classified into the double-layer capacitors which store via a physical adsorption of ions on the surface of the electrodes and pseudocapacitors using a redox reactions mechanism between the active material and the electrolyte.[1] The specific surface area (SSA) and pore size distribution (PSD) are important parameters for analysis of electrode materials for supercapacitors because it has been shown that these properties are linked to the architecture of the material containing different porosity that are desired for effective for optimum performance.[2–5] Based on the above properties, carbon-based materials are the most suitable choice for supercapacitors applications and they have been studied extensively due to their highly porous and adjustable structural properties, conductivity, high SSA and chemical stability.[1] Carbon has a large family of nanostructured materials with either sp^2 or sp^3 allotropes such as activated carbon (AC),[6] nanotubes (CNTs),[7,8] carbide-derived carbons (CDCs),[9,10] onion-like carbons (OLCs)[11,12] and graphene[13,14] with a variety of shapes that are suitable as electrode materials for the next generation of supercapacitor.

Amongst these allotropes, the porous and disordered sp^3 activated carbon is the choice material for commercial applications and is usually produced from fossils fuel or coal tar pitch. However, considering the increasing demand for energy and the gradual consumption of the fossil fuels, there is a need for an alternative source of carbon materials for energy application that is sustainable. Activated carbon can be produced from organic and inorganic precursor materials, previously, we have demonstrated the production activated carbon from a composite of graphene foam, Poly(vinyl alcohol, phenol, and formaldehyde as electrode material for supercapacitors,[15] similarly, activated carbon was produced from a polymer blend of polyvinylpyrrolidone (PVP) and polyvinyl alcohol (PVA) with graphene foam and the physicochemical properties have been elucidated as potential

[a]Corresponding Author: Email address: Ncholu.Manyala@up.ac.za Tel: +27 (0)12 420 3549, Fax: +27 (0)12 420 2516

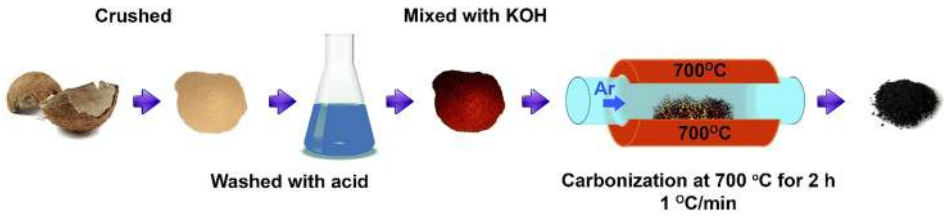

Scheme 1. Synthesis route of CSAC.

electrode materials for supercapacitors.[16] PVA was used because it has exceptional properties and electrochemical stability,[17–19] while PVP has excellent absorption and compound making abilities.[20] Activated carbon was produced from the dispersion of expanded graphite in polyvinylpyrrolidone and the material exhibited a specific surface area of 457 m^2 g^{-1} and a high specific capacitance of 337 F g^{-1}, energy density of 37.9 Wh kg^{-1}, power density of 450 W kg^{-1} and excellent stability voltage holding.[21] This present study is aimed at studying the production of porous carbon material from a natural source such as coconut shell which is due to the fact that natural sources are low cost, abundance, sustainable and sometimes renewable when compared with the organic and inorganic sources. Coconut shell is a lignocellulosic biomass material that can be explored as a sustainable source of porous carbons with its excellent natural structure, high carbon yield, and low ash content which make it suitable for application as an electrode material in EDLCs as reported by various groups.[22–25] Herein, we report on the large scale production of porous carbon derived from coconut shell using a one-step acid treatment, pyrolysis followed by chemical activation. The obtained carbon material was characterized and subsequently used as electrodes for a symmetric supercapacitor device which demonstrated excellent capacitance retention after floating for 100 h.

II. EXPERIMENTAL

Scheme 1 presents the preparation process of the activated carbon derived from coconut shell (CSAC) material. Firstly, 5 g of the coconut shell was crushed and dispersed in 100 ml of acetic acid and the mixture was sonicated for 12 h. The obtained material was washed with deionized water and dried; afterwards 10 g of KOH was then mixed with acid treated material and carbonized at 700 °C at 5 °C/minute, under argon gas atmosphere for 2 h. The carbonized sample was washed with 1 M HCl to remove the remaining KOH, followed by washing with deionized water until a neutral PH was attained and the sample was dried at 60 °C.

III. MATERIALS CHARACTERIZATION

A field emission scanning electron microscope (FE-SEM) was used to study morphology, X-ray diffraction (XRD) and Raman spectroscopy for structural analysis. The surface area studies were carried out a Micromeritics TriStar II 3020 (version 2.00) analyzer. All the samples were degassed at 180 °C under high vacuum for 12 h. The surface area was calculated by the Brunauer–Emmett–Teller (BET) method from the adsorption branch in the relative pressure range (P/P0) of 0.01 - 0.2. All electrodes were prepared according to our similar reports[26] and the electrochemical test of the symmetric cell was carried out in a two electrode cell. A PVA-KOH-CB (PKC) gel previous reported[26] was used as the electrolyte. Our choice of polymer-based gel electrolytes is due to their anticorrosive properties, which makes them compatible with metal current collectors which exhibit good physical contact and good ionic conductivity with good stability.[27,28] All electrochemical measurements were carried out using a Bio-logic VMP-300 potentiostat.

IV. RESULTS AND DISCUSSION

The microstructure of the produced CSAC in Figure 1 (a) shows low magnification micrograph of the sample revealing porous cavities, while Figure 1 (b) higher magnification image features

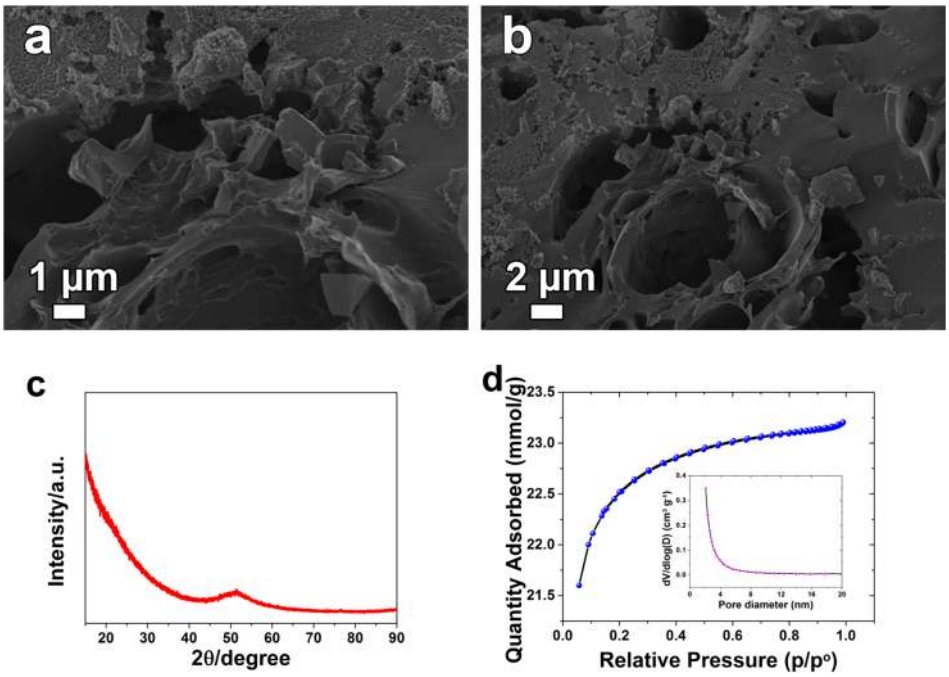

FIG. 1. (a) and (b) high and Low magnification SEM images, (c) the X-ray diffraction and (d) the N_2 adsorption-desorption isotherm of CSAC.

a substantial amount of interlinked micrometric pores in the three-dimensional framework which could be beneficial for charge storage since the porosity governs the performance of the electrode.[29] Figure 1 (c) represents the XRD pattern of the CSAC sample. A weak and broad reflection at 52° is observed and is assigned to the 101 plane of graphite. The wide peak is a hint that the structure of the material is amorphous. Figure 1 (d) presents the obtained results from the gas sorption analysis. The N_2 isotherm display type I properties for the CSAC with a corresponding SSA of 1416 m^2 g^{-1}. The inset to the figure is the pore size distribution (PSD) revealing a predominantly microporous structure with a pore size distribution below 2 nm. The high SSA and small PSD are expected to be beneficial to the performance of the electrode.[30]

To evaluate the performance of the electrode material, symmetric supercapacitor device was fabricated and optimized. The CVs of symmetric cell with a sweep rate of 50 mV s^{-1}at different voltage ranges of 1.1 to 1.5 V is shown in Figure 2 (a) and the CV keeps its symmetric rectangular shape with respect to increasing potential window which indicates the typical electrical double-layer capacitance (EDLC) of the CSAC. Figure 2 (b) shows the CV curves at scan rates between 10 - 100 mV s^{-1} of which the CV shapes still maintain a nearly perfect symmetric rectangular shape, at cell potential of 1.3 V, showing that there was no capacitance decay to the electrode material with increasing sweep rates, and indicating rapid ions transport mechanism with excellent rate capability of the electrode material. The galvanostatic charge-discharge (GCD) curves at different current densities from 0.5 A g^{-1} to 10 A g^{-1} are shown in Figure 2 (c). The GCD curves are triangular and symmetrical in shape, confirming an EDLC behavior with excellent electrochemical reversibility. The corresponding electrode specific capacitance as a function of the current density of the device calculated from the slope of the discharge curve and Ragone plot are shown in Figure 2 (d) based on equations 1 – 3 below:

$$C_{sp} = 4 \times \mathrm{I}\Delta t/m\Delta V \tag{1}$$

$$E_{max} = 0.5C(\Delta V)^2 = (C_{sp} \times \Delta V^2)/28.8 \tag{2}$$

$$P_{max} = 3.6 \times E_{max}/\Delta t \tag{3}$$

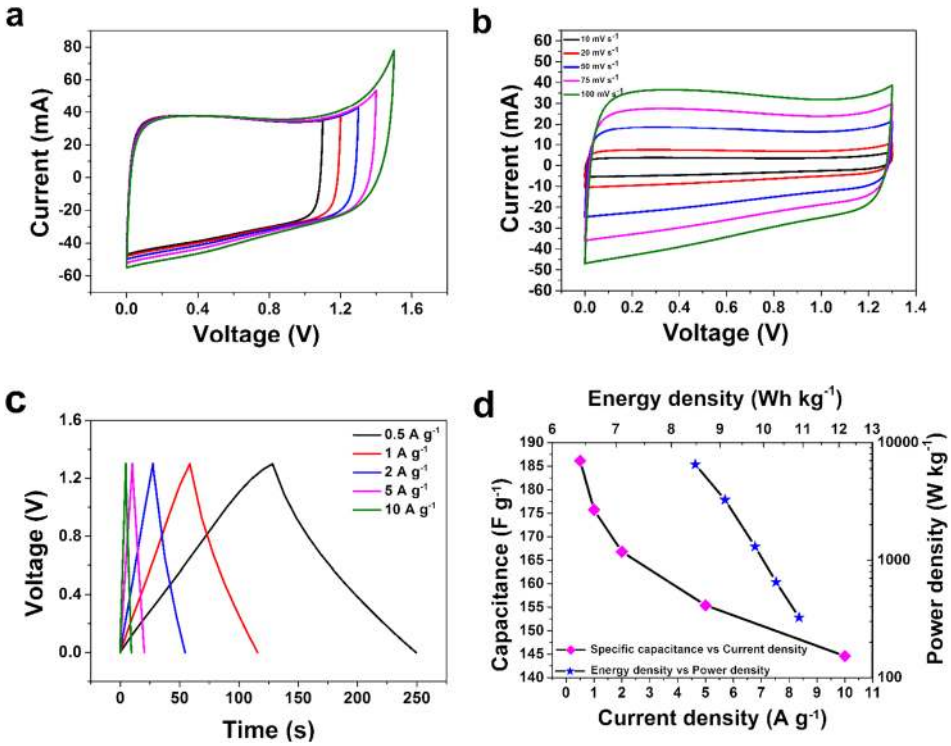

FIG. 2. (a) CV at different voltage windows(100 mV s^{-1}), (b) CV at scan rates at 1.3 V, (c) The GCG curves at different current densities, (d) The specific capacitance, energy and power density as function of the current density of CSAC cell.

Where the specific capacitance in F g^{-1} is given by C_{sp}, E_{max}, energy density (Wh kg^{-1}), P_{max}, the power density (kW kg^{-1}), I is the current (A), m is the mass of the active material (g), Δt is the discharge time (s), and Δv is the potential (V).

The device exhibits a specific capacitance of 186 F g^{-1} at a current density of 0.5 A g^{-1}. At current density as high as 10 A g^{-1}, the device still maintains a specific capacitance value of 144 F g^{-1}, showing only 22.5 % loss to the initial capacitance. Furthermore, the energy and power densities of ~11 Wh kg^{-1} and 325 W kg^{-1} were obtained at current density of 0.5 A g^{-1}. Compared to previous studies on agricultural wastes as carbon sources for EDLCs, this work presents an improvement to present literature for example AC based on coffee shells displayed a specific capacitance of 156 F g^{-1},[31] while a specific capacitance of 79 F g^{-1} was also report for AC obtained from coconut shells with a power density of 170 W kg^{-1} and a specific energy density of 1 Wh kg^{-1} by Zhou *et al.*.[32] Similarly, a specific capacitance of 133.4 F g^{-1} at current density of 0.2 A/g was reported for coconut leaves activated carbon,[33] while microwave-Induced KOH activation of coconut shell produced activated carbon with a surface area and specific capacitance value of 1768.8 m^2 g^{-1} and 156.33 F g^{-1} respectively.[34]

The stability of the device was investigated using continuous GCD and floating (aging) methods[35] as shown in Figure 3. Figure 3 (a) shows the voltage-holding curve for the period of 100 h, which shows no decrease in the specific capacitance values throughout the aging time, signifying that the device exhibited excellent stability and no degradation. The Coulombic efficiency and specific capacitance as a function of the cycle number is shown in Figure 3 (b) and also reveals that the device also exhibited excellent stability after 10000 GCD cycles at 5 A g^{-1} without significant loss of capacitance, suggesting that the continuous cycling do not cause any appreciable structural change of the electrode material. Figure 3 (c) shows the CV curves at 50 mV s^{-1} before and after 10000 cycles which display no appreciable degradation (no change in CV shape) rather, a small decrease in current response was observed after voltage holding and cycling. These CV curves basically indicate that no falloff in the performance of the device, thus supporting the results obtained in Figure 3 (a) and (b).

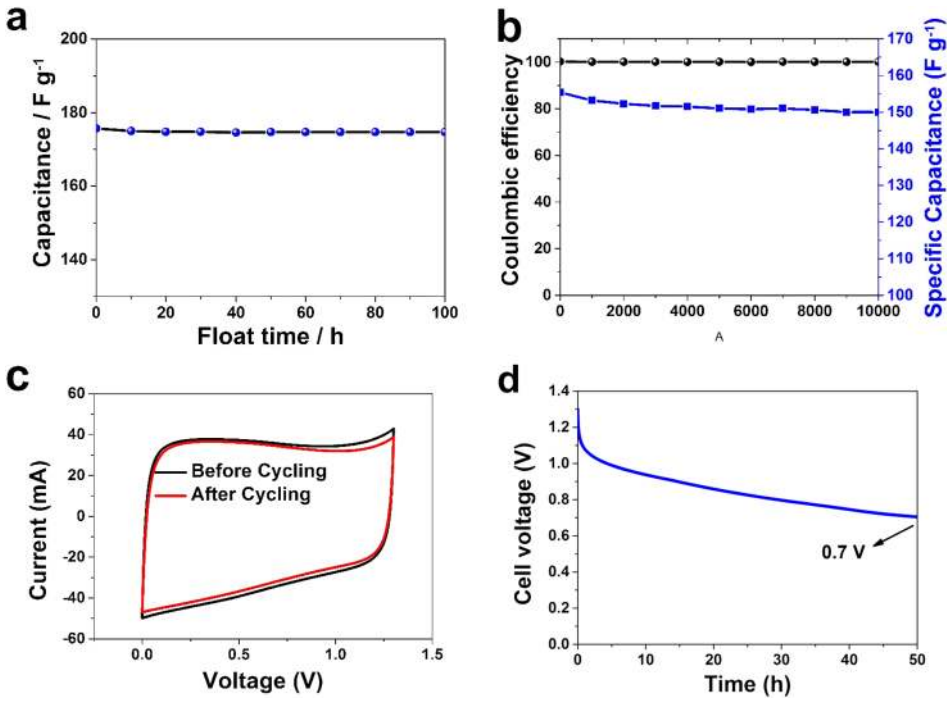

FIG. 3. (a) Floating test as a function of capacitance at of 1 A g^{-1}, (b) Cycle stability at 5 A g^{-1} (c) CV curves at 100 mV s^{-1} before and after 10000 cycling and (d) Self-discharge of the symmetric capacitor curves after the devices were charged at constant current of 1 A g^{-1}.

Self-discharge (SD) of the symmetric cell in gel electrolyte was also investigated at room temperature as shown in Figure 3 (d). The device was charged to its maximum voltage of 1.3 V and held at that voltage for about 1 h and then was kept at open circuit potential to undergo self-discharge for 50 h. The voltage on the capacitor terminals was monitored. The quick drop of the cell voltage at the initial stage of the self-discharge is probably due to the decomposition of the solvent which is water in this case, as explained by Chen *et al.*.[36] Briefly, the solvent can be abridged on the cathode when the device is completely charged. This reduction can go on even after current cut-off, leading to a swift decrease in the cathode potential. This procedure is influenced by the surface property of the electrode and is not diffusion controlled neither due to current leakage. Therefore, any investigation of the self-discharge mechanism will exclude this potential drop.

To establish the major mechanism dictating the self-discharge, two well accepted models were considered. The first model relates the self-discharge of the supercapacitor to current leakage over a resistance R, using equation 4:

$$V = V_0 exp^{(\frac{-t}{RC})} \tag{4}$$

Where V_0 is the initial voltage and C is the equivalent capacity of the device respectively. Thus, the plot of lnV vs t should give a linear trend. However, our result deviates from this linear behavior as shown in the fitting of the data in Figure 4 (a). This implies that the self-discharge observed here is not triggered by current leakage through a resistance. The second model is based on diffusion-control process. In other words, in this model, the accumulated charges are lost due to out-diffusion of the electrolyte ions in the electrical double layer. The voltage drop of this diffusion process is dictated by equation 5:

$$V = V_0 - mt^{1/2} \tag{5}$$

where m is the diffusion parameter and is related to the initial voltage V_0. Our data fit well to this model (see Figure 4 (b)), showing that the dominant mechanism influencing the self-discharge is diffusion of the electrolyte ions from the electrical double layer capacitor.

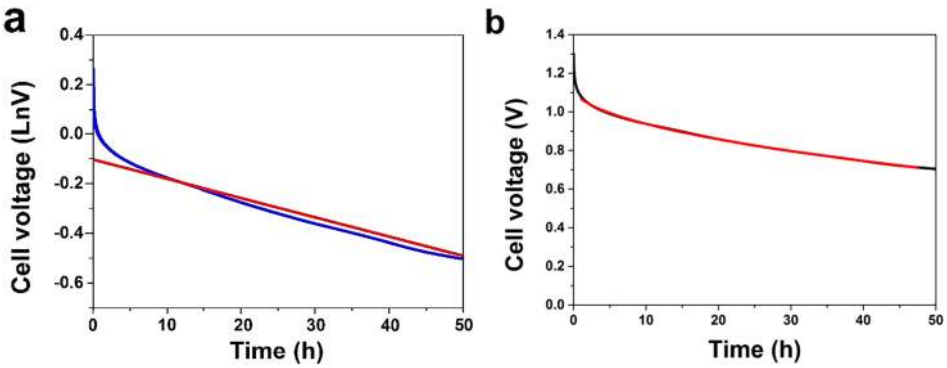

FIG. 4. (a) fitting the self-discharge data with equation 1 and (b) fitting the self-discharge data with equation 2.

The electrochemical impedance spectroscopy of the device was analyzed and the results are shown in Figure 5. Figure 5 (a) shows the Nyquist plot of the device and its corresponding equivalent circuit as an inset. At the high frequency, the intercept on the real Z axis of the Nyquist plot give evidence about the resistance of the electrolyte, the contact, and the electrode materials (R_S). The low R_S (0.43 Ω) of the electrode material reveals good conductivity of the produced carbon materials. The small partial semicircle in the medium-frequency region is due to the charging of the double layer and is assigned to the charge transfer resistance and mass transport across the framework of the porous material, and is shown by R_{CT} and its value is found to be 0.04 Ω. In the low-frequency region, the Nyquist plot shows a nearly vertical line indicating ideal capacitive behavior. The deviation from the perfect vertical line is due to the diffusion of ions at the electrode – electrolyte interface which is usually characterized by the presence of a Warburg impedance characteristic element denoted by W.[37] The inset to the Figure presents the RC circuit. The R_s is linked in series with the double

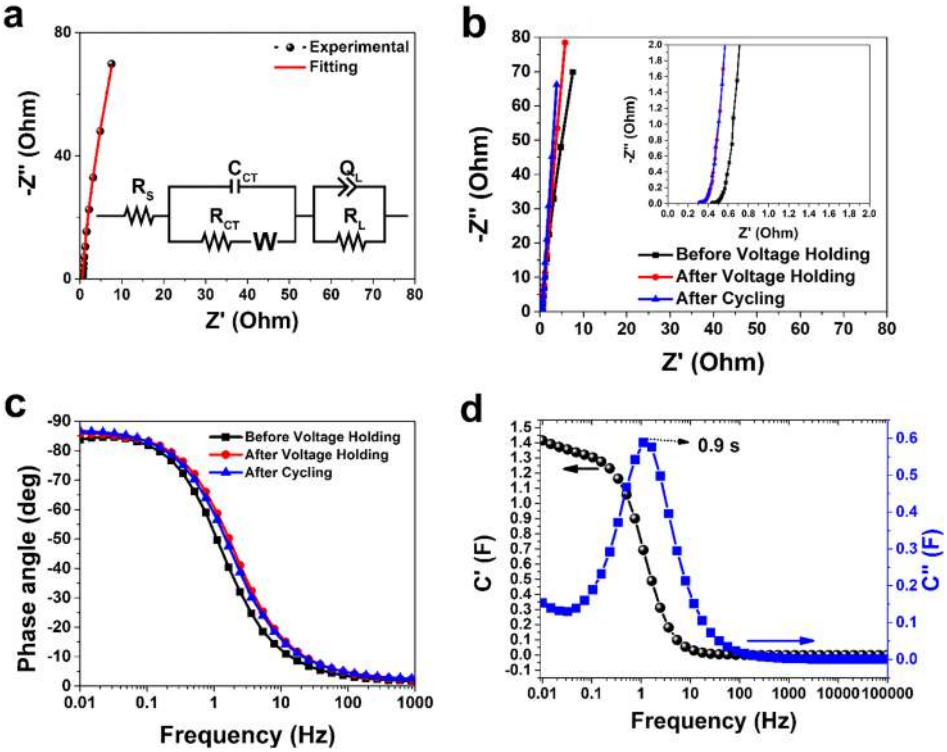

FIG. 5. (a) Nyquist and fitting curve, (b) Nyquist and (c) the phase angle versus frequency, before voltage holding, after voltage holding and after 10000 cycling, and (d) the Z' and the Z" capacitance against frequency.

layer capacitance, which is linked in parallel with the R_{CT}. The changeover from high-low frequency is modeled by Warburg element represented by W which is in series with R_{CT}.

An ideal polarizable capacitive electrode with the mass capacitance should give rise to a straight line parallel to the imaginary axis at low frequency, but from Figure 5 (a) there is a shift from this ideal behavior, ascribed to a resistive element related with the constant phase element Q_L. This resistive element is known as leakage resistance R_L and is in parallel with Q_L. The Nyquist plots were also compared after both floating test and cycling and the result is presented in Figure 5 (b). There is an improvement in the initial R_S value from 0.43 Ω to 0.30 Ω after both voltage holding and cycling. The Bode plot which defines the phase angle for the electrodes is presented in Figure 5 (c) for each stage of characterization namely; before and after both voltage holding and cycling. They all show similar phase angle of ∼-85°, very close to -90° for ideal behavior. The complex capacitance of the device as a function of the frequency before cycling is shown in Figure 5 (d). C' is the real accessible capacitance of the cell that can be delivered and this correspond to a deliverable capacitance of 1.4 F. C" expresses the changeover frequency between a capacitive and a resistive behavior and also depict the energy loss because of the irreversible process of the electrodes.[38] From the figure, C" shows a peak at 1.1 Hz, defining a relaxation time τ of ∼0.9 s from using $\tau = 1/\omega_{max} - 1/2\pi f_{max}$ This indicates that the device can be fully charged within a very short time of 0.9 s.

V. CONCLUSIONS

In summary, activated carbon with a high surface area of 1416 $m^2\ g^{-1}$ was synthesized from coconut shell (CSAC) and provided a great electrochemical performance in the PVA-KOH-CB (PKC) polymer gel electrolyte. The CSAC device shows a high specific capacitance of 186 F g^{-1}, the energy and power densities of ∼11 Wh kg^{-1} and 325 W kg^{-1} respectively at 0.5 A g^{-1}. No significant capacitance loss of the device was noticed after floating for 100 h or after cycling for 10000 cycles and only a voltage decay of 0.6 V in 50 h of self-discharge (SD) was demonstrated by the device. Overall, these results suggest that there is room for great improvement on CSAC based materials in polymer gel electrolyte for high-performance supercapacitor device applications.

ACKNOWLEDGMENTS

"This work is based on the research supported by the South African Research Chairs Initiative of the Department of Science and Technology and National Research Foundation of South Africa (Grant No 97994). Any opinion, finding and conclusion or recommendation expressed in this material is that of the author(s) and the NRF does not accept any liability in this regard". F. Barzegar and D. Y. Momodu acknowledge the University of Pretoria for Postdoctoral fellowship support, while A. Bello acknowledges financial support from NRF through SARChI in Carbon Technology and Materials.

[1] P. Simon and Y. Gogotsi, Nat. Mater. **7**, 845 (2008).
[2] M. Zhi, C. Xiang, J. Li, M. Li, and N. Wu, Nanoscale **5**, 72 (2012).
[3] M. Zhi, F. Yang, F. Meng, M. Li, A. Manivannan, and N. Wu, ACS Sustain. Chem. Eng. **2**, 1592 (2014).
[4] B. Batalla García, A. M. Feaver, Q. Zhang, R. D. Champion, G. Cao, T. T. Fister, K. P. Nagle, G. T. Seidler, B. Batalla García, A. M. Feaver, Q. Zhang, R. D. Champion, G. Cao, T. T. Fister, K. P. Nagle, and G. T. Seidler, J. Appl. Phys. **104**, 14305 (2008).
[5] M. Inagaki, H. Konno, and O. Tanaike, J. Power Sources **195**, 7880 (2010).
[6] Y. Zhai, Y. Dou, D. Zhao, P. F. Fulvio, R. T. Mayes, and S. Dai, Adv. Mater. **23**, 4828 (2011).
[7] S. Dörfler, I. Felhösi, T. Marek, S. Thieme, H. Althues, L. Nyikos, and S. Kaskel, J. Power Sources **227**, 218 (2013).
[8] E. Iyyamperumal, S. Wang, and L. Dai, ACS Nano **6**, 5259 (2012).
[9] Y. Korenblit, M. Rose, E. Kockrick, L. Borchardt, A. Kvit, S. Kaskel, and G. Yushin, ACS Nano **4**, 1337 (2010).
[10] V. Presser, M. Heon, and Y. Gogotsi, Adv. Funct. Mater. **21**, 810 (2011).
[11] P. Simon and Y. Gogotsi, Acc. Chem. Res. **46**, 1094 (2013).
[12] Y. Gao, Y. S. Zhou, M. Qian, X. N. He, J. Redepenning, P. Goodman, H. M. Li, L. Jiang, and Y. F. Lu, Carbon **51**, 52 (2013).
[13] B. G. Choi, M. Yang, W. H. Hong, J. W. Choi, and Y. S. Huh, ACS Nano **6**, 4020 (2012).
[14] L. L. Zhang, R. Zhou, and X. S. Zhao, J. Mater. Chem. **20**, 5983 (2010).
[15] A. Bello, F. Barzegar, D. Momodu, F. Taghizadeh, M. Fabiane, J. Dangbegnon, and N. Manyala, RSC Adv. **4**, 39066 (2014).
[16] F. Barzegar, A. Bello, O. O. Fashedemi, J. K. Dangbegnon, D. Y. Momodu, F. Taghizadeh, and N. Manyala, Electrochim. Acta **180**, 442 (2015).
[17] N. Rajeswari, S. Selvasekarapandian, S. Karthikeyan, C. Sanjeeviraja, Y. Iwai, and J. Kawamura, Ionics (Kiel). **19**, 1105 (2013).

[18] A. K. Swain and D. Bahadur, J. Phys. Chem. C **118**, 9450 (2014).
[19] D. J. T. Hill and A. K. Whittaker, Radiat. Phys. Chem. **80**, 213 (2011).
[20] R. Meena, R. Lehnen, and B. Saake, Cellulose **21**, 553 (2013).
[21] F. Barzegar, A. Bello, D. Momodu, M. J. Madito, J. Dangbegnon, and N. Manyala, J. Power Sources **309**, 245 (2016).
[22] Z. Hu, M. P. Srinivasan, and Y. Ni, Adv. Mater. **12**, 62 (2000).
[23] Z. Hu, M. P. Srinivasan, and Y. Ni, Carbon **39**, 877 (2001).
[24] L. Sun, C. Tian, M. Li, X. Meng, L. Wang, R. Wang, J. Yin, and H. Fu, J. Mater. Chem. A **1**, 6462 (2013).
[25] A. Jain, V. Aravindan, S. Jayaraman, P. S. Kumar, R. Balasubramanian, S. Ramakrishna, S. Madhavi, and M. P. Srinivasan, Sci. Rep. **3**, 3002 (2013).
[26] F. Barzegar, J. K. Dangbegnon, A. Bello, D. Y. Momodu, A. T. C. Johnson, and N. Manyala, AIP Adv. **5**, 97171 (2015).
[27] H. Yu, J. Wu, L. Fan, K. Xu, X. Zhong, Y. Lin, and J. Lin, Electrochim. Acta **56**, 6881 (2011).
[28] P. Yang, W. Cui, L. Li, L. Liu, and M. An, Solid State Sci. **14**, 598 (2012).
[29] C. Liu, F. Li, L. P. Ma, and H. M. Cheng, Adv. Mater. **22**, E28 (2010).
[30] A. G. Pandolfo and A. F. Hollenkamp, J. Power Sources **157**, 11 (2006).
[31] M. R. Jisha, Y. J. Hwang, J. S. Shin, K. S. Nahm, T. Prem Kumar, K. Karthikeyan, N. Dhanikaivelu, D. Kalpana, N. G. Renganathan, and A. M. Stephan, Mater. Chem. Phys. **115**, 33 (2009).
[32] P. W. Zhou, B. H. Li, F. Y. Kang, and Y. Q. Zeng, **21**, 125 (2006).
[33] K. S. Sulaiman, A. Mat, and A. K. Arof, Ionics (Kiel). **22**, 911 (2016).
[34] M. I. M. Nayai, K. Ismail, M. A. M. Ishak, N. Zaharudin, and W. I. Nawawi, Appl. Mech. Mater. **835**, 289 (2016).
[35] P. Ratajczak, K. Jurewicz, and F. Béguin, J. Appl. Electrochem. **44**, 475 (2013).
[36] L. Chen, H. Bai, Z. Huang, and L. Li, Energy Environ. Sci. **7**, 1750 (2014).
[37] H. Li, J. Wang, Q. Chu, Z. Wang, F. Zhang, and S. Wang, J. Power Sources **190**, 578 (2009).
[38] P. L. Taberna, P. Simon, and J.-F. F. Fauvarque, J. Electrochem. Soc. **150**, A292 (2003).